LBNL-39788
UC-414

ERNEST ORLANDO LAWRENCE
BERKELEY NATIONAL LABORATORY

Study on a Test of Optical Stochastic Cooling Scheme in a Single Pass Beam Line

S. Chattopadhyay, C. Kim, D. Massoletti,
A. Zholents, M. Zolotorev, and W. Wan
Accelerator and Fusion Research Division

January 1997

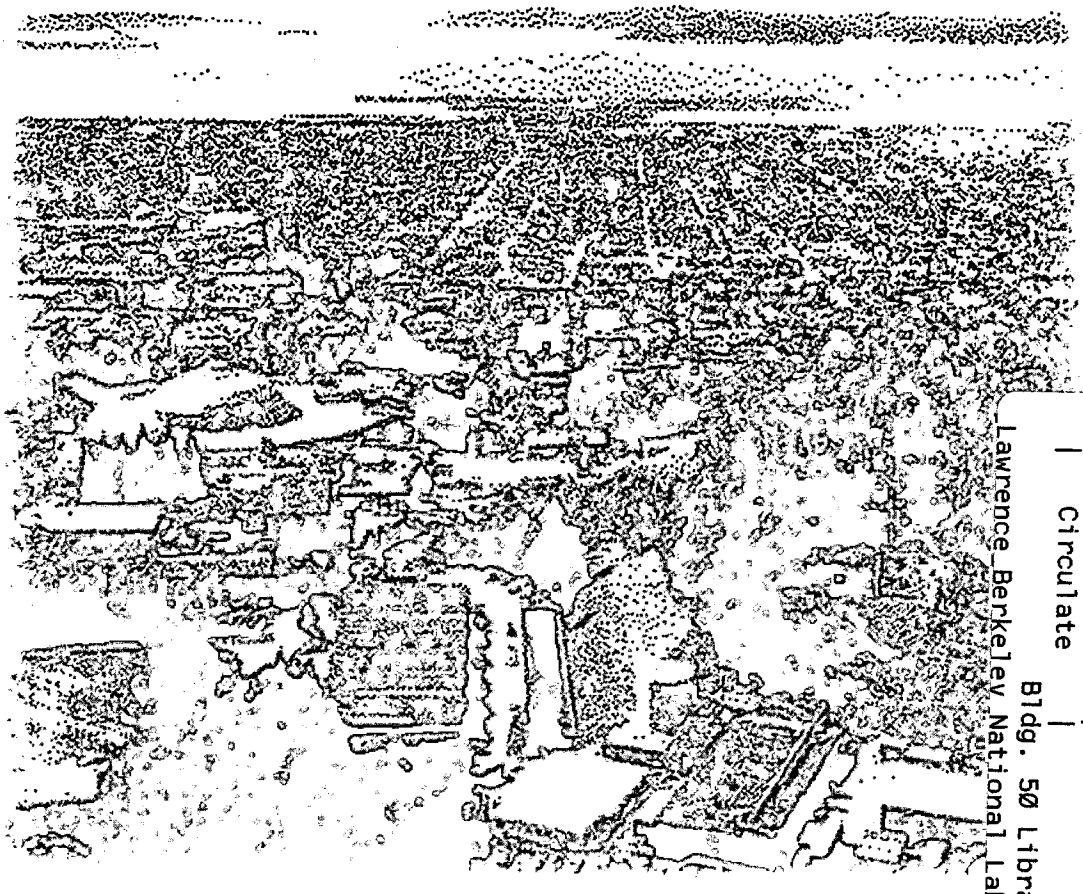

DISCLAIMER

LBNL-39788
CBP Note - 203

Study on a Test of Optical Stochastic Cooling Scheme in a Single Pass Beam Line*

S. Chattopadhyay, C. Kim, D. Massoletti, A. Zholents and M. Zolotorev

Accelerator and Fusion Research Division,
Lawrence Berkeley National Laboratory, University of California,
Berkeley, California 94720

W. Wan

University of Colorado, Boulder, CO 80309

January 1997

*This work was supported by the Director, Office of Energy Research, Office of High Energy and Nuclear Physics, Division of High Energy Physics, of the U.S. Department of Energy under Contracts No. DE-AC 03-76SF00098 and No. DE-FG 03-95ER40926.

1 Introduction

A feasibility study of an experiment to test the principle of optical stochastic cooling [1], [2] is presented. We propose to build a new beamline in the extraction area of the ALS Booster synchrotron, where we will include a bypass lattice similar to the lattice that could be used in the cooling insertion in a storage ring. Of course, in the single pass beamline we cannot achieve cooling, but we can test all the functions of the bypass lattice that are required to achieve cooling in a storage ring. As it is stated in [1], there are stringent requirements on the time-of-flight properties of the bypass lattice employed in a cooling scheme. The pathlengths of particle trajectories in the bypass must be fairly insensitive to the standard set of errors that usually affect the performance of storage rings. Namely, it is necessary to preserve all fluctuations in the longitudinal particle density within the beam from the beginning to the end of the bypass lattice with the accuracy of $\lambda/2\pi$, where λ is the carrying (optical) wavelength. According to [2], cooling will completely vanish if a combined effect of all kinds of errors will produce a spread of the pathlengths of particle trajectories larger than $\lambda/2$ and the cooling time will almost double if the spread of the pathlengths is $\lambda/2\pi$. At a first glance, $\lambda/2\pi \simeq 0.1\mu$m is such a small value that satisfying this accuracy looks nearly impossible. However, simulations show that a carefully designed bypass can meet all the requirements even with rather conservative tolerance to errors.

Although at this point we are sure in our simulations, we think that having done only simulations is not enough to begin a full scale (presumably expensive) testing of optical stochastic cooling in a storage ring. Therefore, we propose to proceed first with a relatively inexpensive experiment in the single pass beamline. This experiment will give us a remarkable opportunity to learn how to handle a difficult problem of time-of-flight operation at a record accuracy. More specifically, we plan to do the following:

1. Define the method to control geometrical and chromatic aberrations of magnetic elements on the particle's pathlengths in the beamline lattice.

2. Define the tolerances for the alignment, tilts and multipole errors of magnetic elements of the beamline.

3. Define the tolerances for the calibration errors of magnetic elements, power supply ripple, and beam orbit fluctuations.

4. Develop a technique for a beam based correction of pathlength errors.

5. Develop a diagnostic technique suitable for measurements of the time-of-flight properties of the beamline lattices.

2 General information

As we have already mentioned, the experimental beamline will be installed in the extraction area of the ALS booster synchrotron. This synchrotron is idle all the time

between injection cycles into the ALS and, thus, available as a source of electrons for a new beamline. We are planing to use electrons at 200-250 MeV energy which is easily attainable in the booster. The layout of the experimental area, showing several Booster synchrotron magnets, the existing beam transport line from the synchrotron to the ALS, and a schematic of a proposed new beamline, is shown in Figure (1).

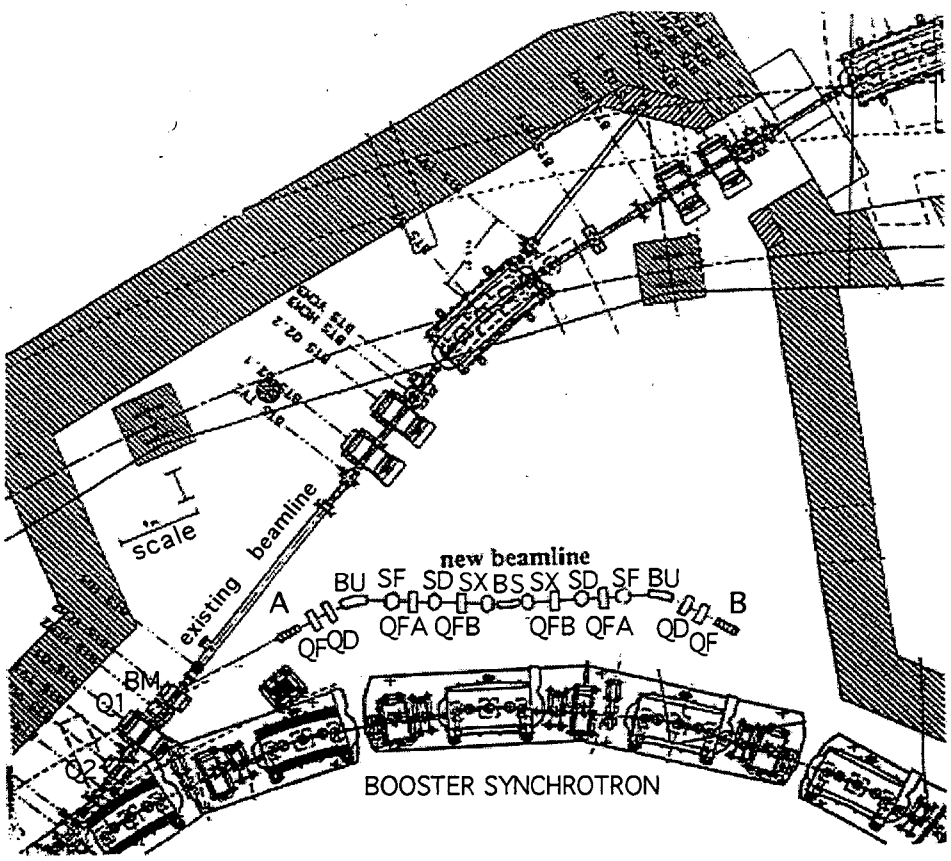

Figure 1: The layout of the extraction area of the ALS Booster synchrotron showing several Booster synchrotron magnets, the existing beam transport line and a schematic of a proposed new beamline.

A proposed beamline has three parts: the beam transport line running from the synchrotron to the bypass lattice (BTL), the bypass lattice itself spanning between undulators A and B, and the beam dump.

The BTL is composed of two quadrupole lenses Q1 and Q2 and one dipole magnet BM. This beamline will be used as a beam transport from the synchrotron to the bypass and for the matching of the beam spot size in the undulator with a diffraction limited size of the undulator radiation. The beginning of this beamline coincides with the existing beam transport line and employs the existing quadrupole Q1. The new quadrupole Q2 replaces the vertical steering magnet K1 which can be relocated downstream of BM.

3 Operation of the Booster synchrotron for beam extraction at low energies

The main mode of operation of the ALS Booster synchrotron is an acceleration of electrons from 50 MeV to 1.5 GeV and injecting them into the storage ring. A typical filling time of the storage ring is approximately 10 minutes. After filling the storage ring, the Booster remains idle for about 2 – 5 hours depending upon the regime of the storage ring operation. During this time the Booster is available for other experiments.

For the experimental test of optical stochastic cooling we need a beam energy only of 200 – 250 MeV. But there are specific requirements on a quality of the beam. In order to get a good quality beam extracted from the Booster at such a low energy, we modified the energy ramp profile in the Booster. Namely, we ramp the beam energy up from 50 MeV to 600 MeV, gives the beam time to stay at this energy, and ramp the beam energy down to about 200 MeV. The goal of this manipulations is to cool the beam emittance and energy spread by using synchrotron radiation damping at the energy of 600 MeV, where the damping time of betatron oscillations is approximately 120 ms. This modification of the Booster operation was done by adding a few extra circuits to the Booster magnet power supply and to the Booster timing system. It takes approximately 10 minutes to switch from the default mode of operation to the modified ramp.

The analysis of the beam parameters achieved after performing the modified ramp showed that at the energy of 250 MeV we can get a beam with the horizontal and vertical emittances of 1.5×10^{-7} m·rad and 1×10^{-8} m·rad correspondent (assuming 6% coupling), and with the energy spread of 7×10^{-4}.

Experimentally, we worked with two ramp configurations shown in Figure (2). In the first configuration, Figure (2a), we kept the beam at the flat top for approximately 1.5 damping times (180 ms). In the second configuration, Figure (2b), we kept the beam at the flat top for 2.8 damping time (330 ms). In the first configuration beam parameters were measured for the beam extracted from the Booster at the energies 250 MeV and 213 MeV. In the second configuration only 250 MeV beam extraction energy was used. Measurements of the beam parameters were performed by extracting the beam from the Booster and observing the variation of the beam profile at the beam profile monitor as a function of the quadrupole strength located upstream of the monitor. The results of these measurements are shown in Table 1. The calculated values are presented in Table 2. One can see, that calculated emittances are systematically lower than the measured values.

As the bench mark test of the measurement technique, we also performed measurements of the beam parameters in the main mode of operation when the beam is extracted from the Booster at 1.5 GeV. The results of these measurements and calculated values are shown in Table 3. Here, again, the calculated horizontal emittance is smaller than as measured. (The calculated vertical emittance was adjusted by varying the coupling, which was also done in a case of low energy extraction).

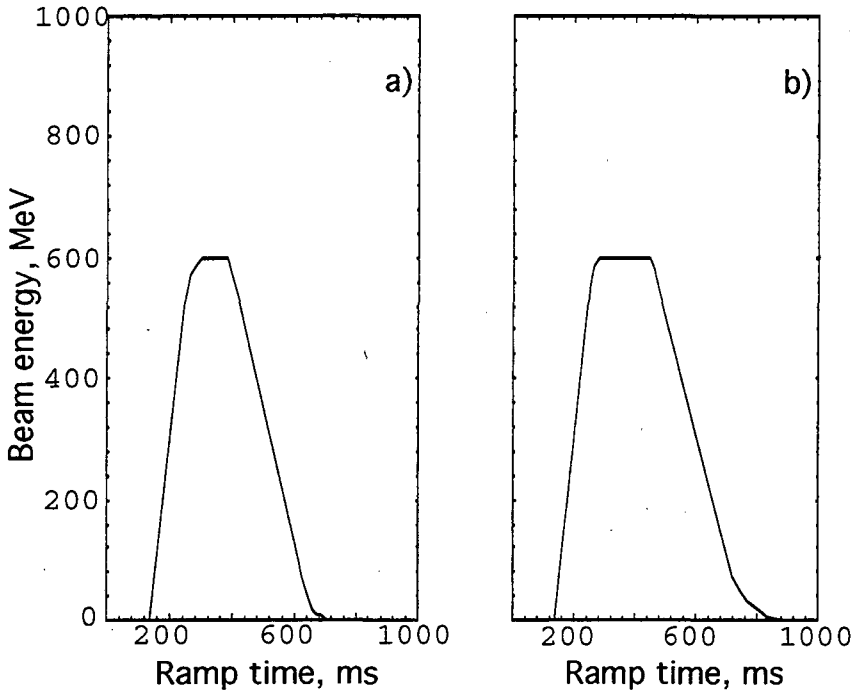

Figure 2: The modified energy ramp of the ALS Booster synchrotron: a) flat top time is 180 ms, b) flat top time is 330 ms.

Table 1: Measured beam parameters for a beam extracted from the ALS Booster at a low energy.

Beam energy [MeV]	213	250	250
Flat top time [ms]	180	180	330
Hor. emittance [m·rad]	$1.6 \times 10^{-7} \pm 26\%$ [a]	$1.25 \times 10^{-7} \pm 22\%$	$1.1 \times 10^{-7} \pm 18\%$
Ver. emittance [m·rad]	$9 \times 10^{-8} \pm 20\%$	$6 \times 10^{-8} \pm 10\%$	$6 \times 10^{-8} \pm 12\%$
Energy spread	$1.5 \times 10^{-3} \pm 26\%$	$\leq 7 \times 10^{-4}$ [b]	$\leq 7 \times 10^{-4}$ [b]

[a] Statistical error. (Systematic error is estimated to be approximately 25%).

[b] The measurement technique was not sensitive to the beam energy spread below this value.

Table 2: Calculated beam parameters for a beam extracted from the ALS Booster at a low energy.

Beam energy [MeV]	213	250	250
Flat top time [ms]	180	180	330
Hor. emittance [m·rad]	0.95×10^{-7}	0.81×10^{-7}	0.53×10^{-7}
Ver. emittance [m·rad]	6.3×10^{-8}	5.4×10^{-8}	2.8×10^{-8}
Energy spread	6.7×10^{-4}	6.1×10^{-4}	7.5×10^{-4}

Table 3: Beam parameters for a beam extracted from the ALS Booster at 1.5 GeV.

Parameter	Measured	Calculated
Hor. emittance [m·rad]	$2.5 \times 10^{-7} \pm 20\%$ [a)]	1.6×10^{-7}
Ver. emittance [m·rad]	$2 \times 10^{-8} \pm 15\%$	2×10^{-8}
Energy spread	$7 \times 10^{-4} \pm 20\%$	6.5×10^{-4}

[a)] Statistical error.

4 Bypass lattice

As it is discussed in [1], [2], the bypass lattice must be highly isochronous for optical stochastic cooling. This requires that the beamline be an achromat and the dependence of the path lengths of electrons from energy, coordinate and angular deviations vanish. Theoretically, an achromat of the second order and higher can be made [3], [4]. In practice, this has been proven to be impossible for this experiment due to the tight space constraint in the proposed experimental area. Taken into account a space needed for matching beamline, undulators, diagnostics, and beam dump, there is approximately only 6m for the bypass lattice. It is too little for a standard second order achromat. Therefore, we designed a modified version of a second order achromat, where all second order aberrations are made small, but not vanish completely. In this design, we aimed at finding a first-order achromat with week second and higher order aberrations and large tolerances to errors.

4.1 Linear optics

As shown in Figure (1), the bypass lattice is mirror symmetric about the center. It contains one combined function magnet in the center, two approximately parallel faced dipole magnets, eight quadrupoles and four sextupoles. All elements of the same kind are identical. The list of elements with definitions of the type, length, and magnetic strengths is given in Table 4.

Table 4: List of elements of the bypass for beam energy 250 MeV.

Element	Length(cm)	Dipole(kG)	Gradient(kG/cm)	Sextupole(kG/cm^2)
Bending magnets				
BU	30	14.55	0	0
BS	30	2.4	0.333	0
Quadrupoles				
QF	9	0	-1.642	0
QD	9	0	0.972	0
QFA	9	0	-1.148	0
QFB	9	0	-0.620	0
Sextupoles				
SF	15	0	0	0.068
SD	15	0	0	-0.052
SX	15	0	0	0.018

The following constraints were imposed in a design. To realize the isochronicity, the R_{51}, R_{52} and R_{56} elements of the linear transport matrix (in TRANSPORT [5] notation)

have to vanish simultaneously. The horizontal electron beam size in the undulator is larger than a diffraction limited size of the undulator radiation. Thus, maintaining the coherence between radiation fields of two undulators requires that no mixing of electron positions occurs in the horizontal plane. This condition entails that linear transport matrix in the horizontal plane be I matrix or $-I$ matrix. It is also convenient to have I or $-I$ linear transport matrix in the vertical plane and $\alpha_x = \alpha_y = 0$ in the undulator center. Besides, the beam size and angular spread in the undulator must be matched to the size and angular spread of undulator radiation, which is achieved by a proper choice of beta-functions in the undulator center. The BTL is designed to satisfy this condition producing $\alpha_x = \alpha_y = 0$, $\beta_x = 1.28$m and $\beta_y = 1.36$m in the center of the undulator. The mirror symmetry of the bypass requires that $\alpha_x = \alpha_y = 0$ in the center of the bypass. Therefore, all together, seven independent knobs are needed to fit the equal number of objective functions in the linear lattice: $\mu_{x,y}$, $\beta_{x,y}$, R_{51}, R_{52} and R_{56}. Notice, that in order to cancel R_{56} a combined function magnet BS bends the beam in the opposite direction of the other two magnets.

After comparing different choices, we choose $\mu_x = 1$ and $\mu_y = 0.5$. The strengths of the four quadrupoles, the edge angles of two dipole magnets and the combined function magnet, and the quadrupole gradient in the combined function magnet were used to find a solution. This was done first in a model without fringe fields and, then, with fringe fields. The solution without fringe fields was obtained by using MAD. Beta-functions and dispersion function of the BTL and the bypass lattice for this solution are shown in Figure (3). The solution with fringe field was obtained using COSY INFINITY [6] for three different models of the fringe fields. These models are (i) the hard edge model, which is quick but not highly accurate; (ii) the Enge model, which is accurate but very slow; and (iii) the symplectic scaling model, which is rather accurate and much faster than the Enge model. Solutions based on all three models were different from each other. But, further cross checking of the solutions showed that the main parameters of the solution found without fringe fields are not sensitive to any specific model. For example, the changes of the tunes and beta-functions from model to model are below 1%, which is well below the tolerances to the bypass lattice. As for the time-of-flight parameters (matrix coefficients R_{51}, R_{52} and R_{56}), we found that on a level of 0.1μm they are more sensitive to the specific model of the fringe fields. For example, the discrepancy between the Enge model and the symplectic scaling model were well below the 0.1μm tolerance, but the discrepancy between the Enge mode and the hard edge model were a few times greater than 0.1μm. Yet this is not a vital problem, since by tuning the quadrupoles we were able to get desired time-of-flight parameters in all three models. Moreover, if necessary, mapped field data can be used in COSY INFINITY to find the new solution. Therefore, the symplectic scaling model and the solution corresponding to it are used throughout the report.

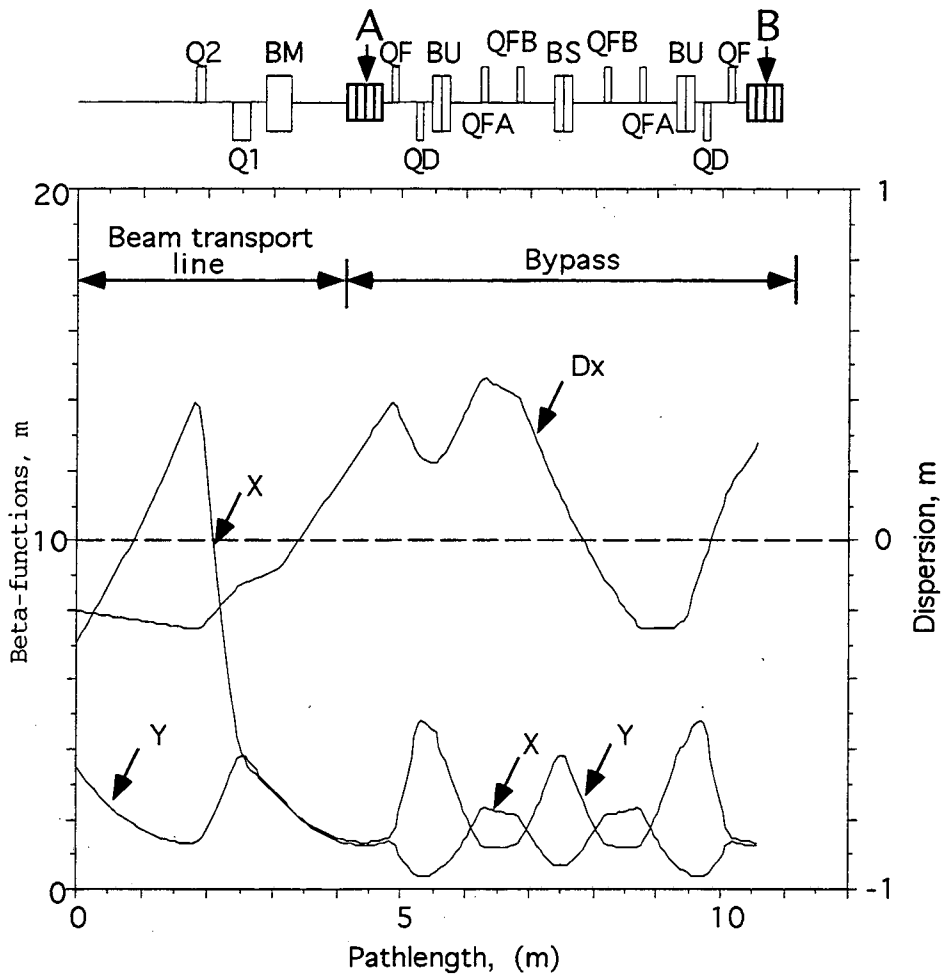

Figure 3: The beta-functions and the dispersion function of the BTL and the bypass lattice.

4.2 Correction of the aberrations

After the careful selection of the first-order solution, aberrations above the second order become negligible and the second-order aberrations become weak. To minimize the remaining second-order aberrations, six sextupoles are placed symmetrically in the bypass. The three independent sextupole strengths are fitted to minimize nine second-order time-of-flight matrix elements: T_{511}, T_{512}, T_{522}, T_{533}, T_{534}, T_{544}, T_{516}, T_{526}, T_{566} (in TRANSPORT notation). Each matrix element was considered to be small if the pathlength deviation associated with this coefficient at the end of fitting procedure fell below 0.1μm. As a result, the ideal lattice, i.e. the lattice without errors, met all the constraints.

5 Simulation results

In order to have a detailed check of the isochronicity of the bypass lattice with errors we performed a 'brute-force' particle tracking using COSY INFINITY. In all simulations we looked at the spread of the longitudinal coordinates of 10^4 electrons after passage through bypass lattice. The electrons entered the lattice at the same time, but had distributions in energy, transverse coordinates and angles. We assumed that all beam distributions are Gaussian and correspond to the measured beam parameters listed in Table 5. All errors were assumed to obey Gaussian distributions truncated at $\pm 2.5\sigma$, where σ is the standard deviation of the distribution.

Table 5: The list of beam parameters.

Beam energy, MeV	250
Horizontal emittance, m·rad	1.1×10^{-7}
Vertical emittance, m·rad	6×10^{-8}
Energy spread, σ_E	7×10^{-4}
Twiss parameters	
β_x, m	1.28
α_x	0
β_y, m	1.36
α_y	0
Beam sizes	
σ_x, m	4.4×10^{-4}
$\sigma_{x'}$, rad	3.4×10^{-4}
σ_y, m	1.2×10^{-4}
$\sigma_{y'}$, rad	8.6×10^{-5}

At the beginning, we produced a spread of the pathlength for an ideal lattice without errors. The result of simulations with and without sextupoles correcting second order

aberrations is shown in Figure (4). Obviously, for beam parameters specified in Table 5, the implementation of sextupole correction is absolutely essential.

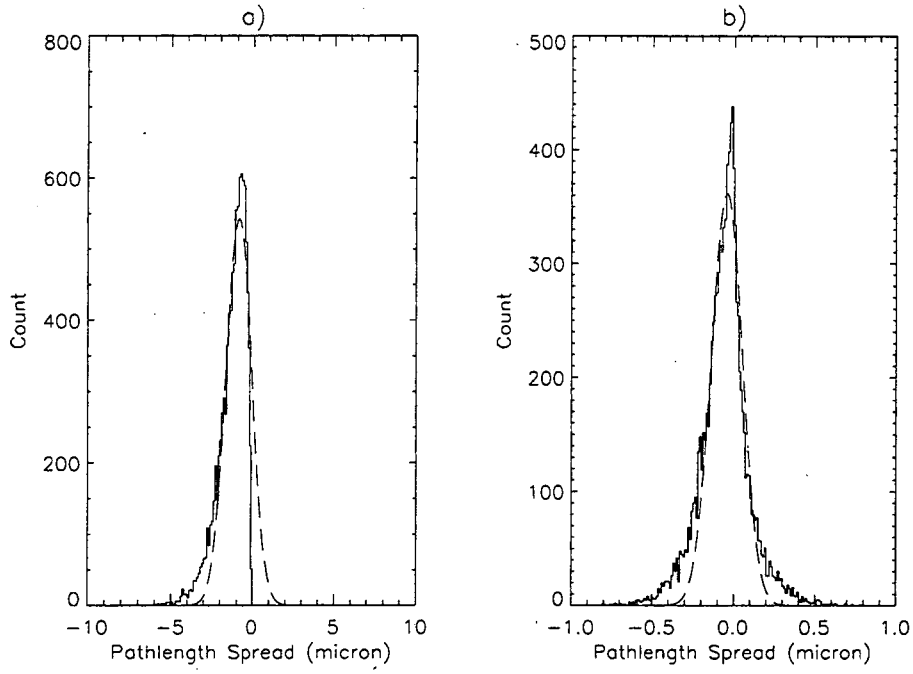

Figure 4: Histograms showing a spread of the pathlengths for the ideal lattice: a) without sextupole correction ($\sigma = 0.74$ μm), b) with sextupole correction ($\sigma = 0.09$ μm). Here and in the subsequent similar pictures all sigmas are given for a fitted Gaussian distribution, which is shown by the dashed line. Note, that a scale of the horizontal axis is ten times larger for the first histogram.

A closer look at the different kinds of errors shows that they can be divided into two categories. The first category consists of errors that are of a static nature, i.e. remain unchanged over a long period of time. These errors are the setting errors, i.e. errors that appeared in manufacturing, assembly and calibration of the magnets, the multipole errors, and the misalignment errors including magnet tilts.

The second category of errors is of a dynamic nature. It includes power supply ripple and beam energy jitter and errors in the coordinates and angles at the entry of the bypass lattice.

Table 6 contains all the errors that are included in the simulations.

Table 6: The specification of the errors.

	Static errors
Setting errors	$\sigma(\frac{\Delta B}{B}) = 1 \times 10^{-3}$ and the same for quadrupoles and sextupoles
Tilt errors, mrad	$\sigma(\Delta\psi) = 0.2$
Misalignment errors	
in x, μm	$\sigma(\Delta x) = 150$
in y, μm	$\sigma(\Delta y) = 30$
in z, mm	$\sigma(\Delta z) = 1$
Multipole error	
dipoles	$\sigma(\frac{b_3}{b_1}) = 1 \times 10^{-4}$ at $r = 3$cm [a)]
quadrupoles	$\sigma(\frac{b_3}{b_2}) = 5 \times 10^{-4}$ at $r = 5$cm [a)]
	Dynamic errors
Position jitter	equal to 1/3 of the beam size in coordinates and angles
Energy jitter	$\sigma = 0.5\%$
Power supply ripple	$\sigma(\frac{\Delta B}{B}) = 1 \times 10^{-4}$ and the same for quadrupoles and sextupoles

[a)] b_1, b_2 and b_3 are the dipole, quadrupole and sextupole components of the magnetic field

The static errors are larger than the dynamic errors, but they can be corrected to a certain extend using a beam based correction technique. For example, as soon as static errors were added to the bypass lattice, the pathlength spread rose to about 1μm, i.e. about one order of magnitude larger than it is acceptable (see, the histogram in Figure (5a)). This growth was mainly attributed by the effect of the mismatching of the linear lattice. Tuning two families of quadrupoles, excited symmetrically and asymmetrically, allowed us to reduce the spread to around 0.1μm (see, the histogram in Figure (5b)).

The effect of the dynamic errors is more severe, since they change each time the beam passes the bypass lattice. Therefore, we carefully studied each kind of the dynamic error by adding them individually to the same set of the static errors already used to correct for the linear mismatching effect. Among the static errors, only multipole errors were not included in these simulations, because they are not corrected like the others. The results of these simulations for two seeds are shown in Figures (6) — (8). As seen in these histograms, there is no any dominant type of dynamic error. For the error specifications,

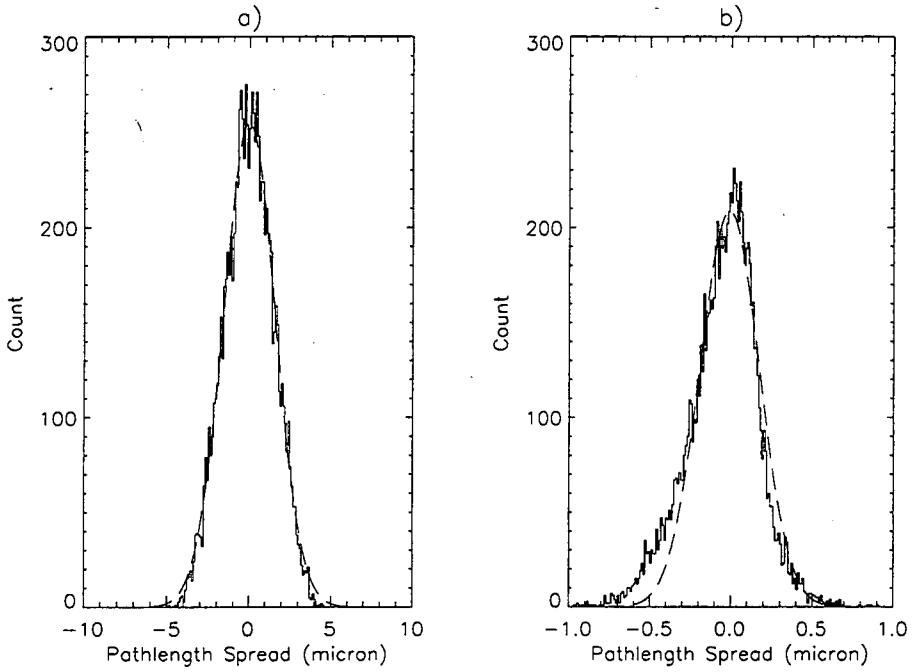

Figure 5: Histograms showing a spread of the pathlengths due to the static errors: a) before correction ($\sigma = 1.57\mu$m), b) after correction ($\sigma = 0.181\mu$m). Note, that a scale of the horizontal axis is ten times larger for the first histogram.

shown in Table 6, contributions of all kinds of dynamic errors are comparable.

Figure (9) demonstrates the individual contribution of the multipole errors in addition to all other static errors.

A combined effect of all dynamic and static errors is shown in Figure (10). Analysis of these histograms will be done in the next section.

Since the tolerance imposed on the misalignment error in the y-direction is tight, we performed the simulation with the five times relaxed tolerance, namely, $\sigma(\Delta y) = 150\mu$m. The corresponding histograms for two seeds are shown in Figure (11). A large spread of the pathlengths appearing here is due to the effect of mismatching of the linear lattice in the vertical plane. The bypass lattice in the present form has no knobs to correct this mismatching, since there is no space in the extraction area of the Booster synchrotron to add more elements into the lattice. Therefore, the tight tolerance for vertical alignments must be observed.

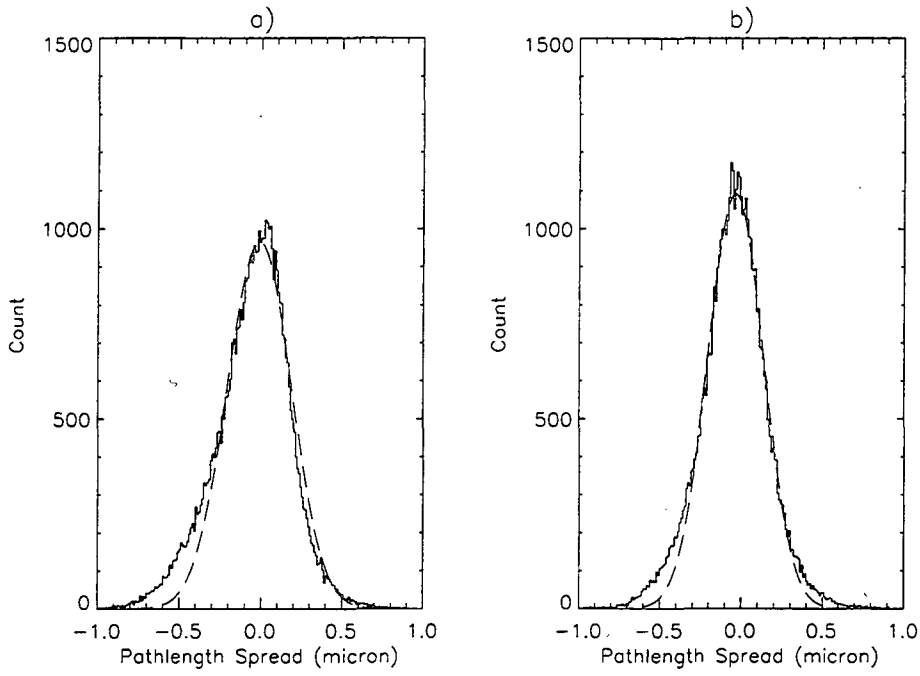

Figure 6: Histograms showing a spread of the pathlengths due to the static errors after correction plus the position jitter of the beam coordinates and angles: a) first seed (σ = 0.194 μm), b) second seed (σ = 0.170 μm).

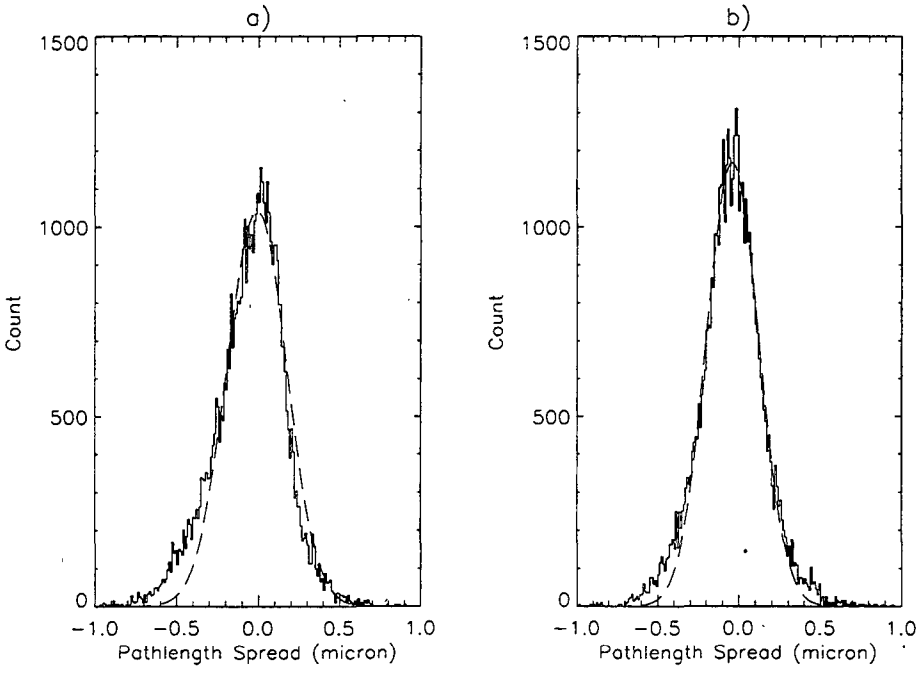

Figure 7: Histograms showing a spread of the pathlengths due to the static errors after correction plus energy jitter: a) first seed (σ = 0.181 μm), b) second seed (σ = 0.158 μm).

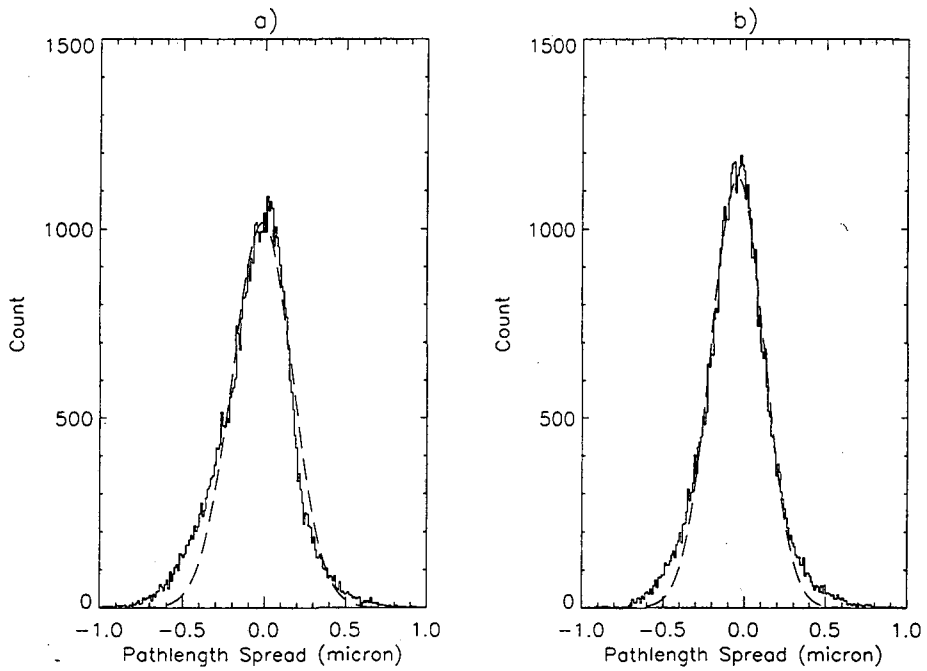

Figure 8: Histograms showing a spread of the pathlengths due to the static errors after correction plus symmetric power supply ripple: a) first seed ($\sigma = 0.184$ μm), b) second seed ($\sigma = 0.161$ μm).

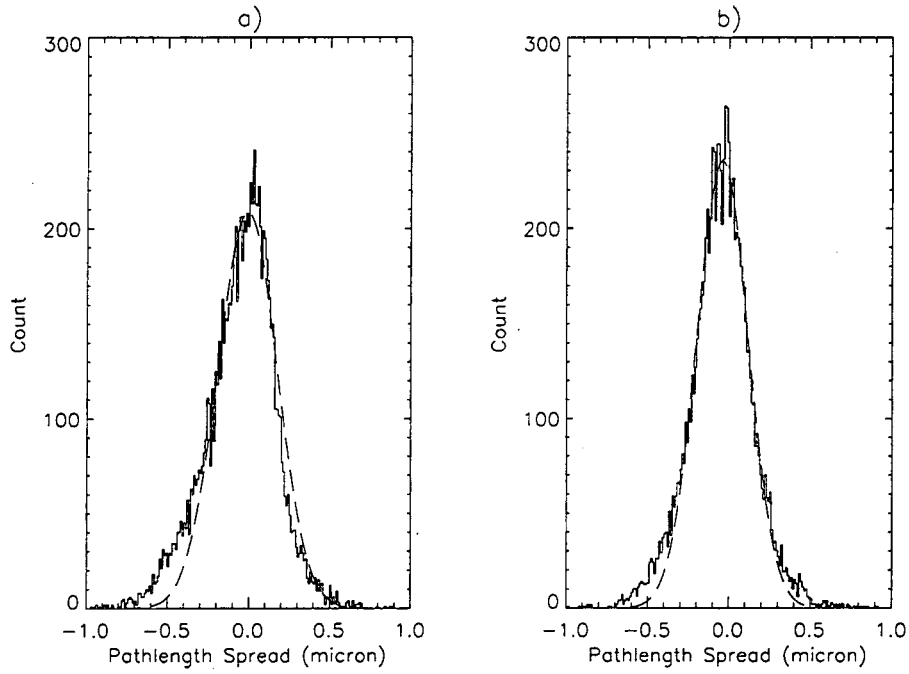

Figure 9: Histograms showing a spread of the pathlengths due to the all static errors including multipole errors after correction: a) first seed ($\sigma = 0.181$ μm), b) second seed ($\sigma = 0.157$ μm).

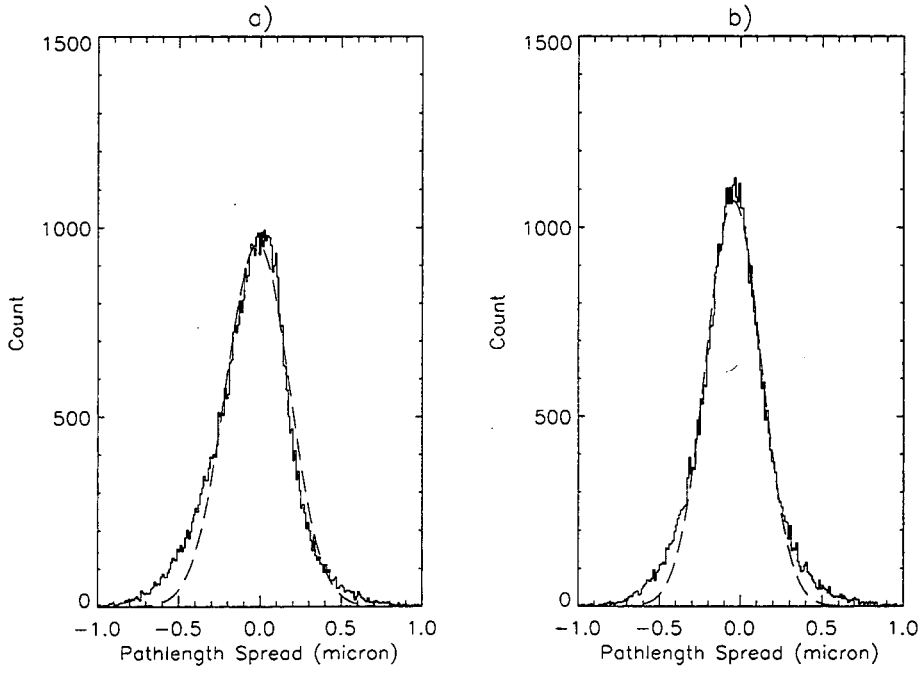

Figure 10: Histograms showing a combined effect of all static errors after correction and all dynamic errors: a) first seed ($\sigma = 0.194$ μm), b) second seed ($\sigma = 0.169$ μm).

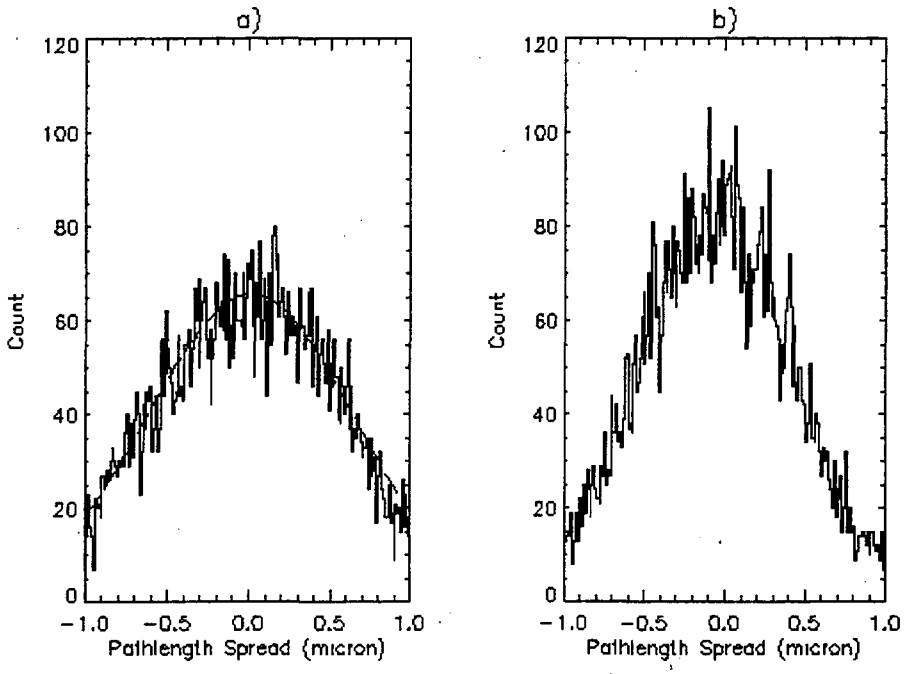

Figure 11: Histograms showing a spread of the pathlengths due to the static errors with correction when a 150μm vertical misalignment error is assumed: a) first seed (σ = 0.630μm), b) second seed (σ = 0.487μm).

6 Analysis

In this section we perform a quantitative analysis of the effect of time-of-flight errors. For this purpose we find a degree of coherence of radiation fields of two undulators, which in normalized form can be characterized by a dimensionless correlation function:

$$\gamma_{12}(\tau) = \frac{\langle E_1(t)\, E_2^*(t+\tau)\rangle}{\left[\langle |E_1(t)|^2\rangle \langle |E_2(t)|^2\rangle\right]^{1/2}}, \tag{1}$$

where γ_{12} is the correlation function, $E_1(t)$ is the far field beam radiation at the first undulator, and $E_2(t)$ is the far field beam radiation at the second undulator. Averaging, denoted by the brackets $\langle ... \rangle$, involves integration over the large time interval.

The radiation field of the electron bunch in a short undulator is built up from the radiation of the individual electrons $e(t)$:

$$E_{1,2}(t) = \sum_{i=1}^{N} e\left(t - \tau_i^{(1,2)}\right), \tag{2}$$

where N is the number of electrons in the electron bunch, $\tau_i^{(1)}$ is the time of the radiation for the ith electron in the first undulator and $\tau_i^{(2)}$ is the time of the radiation for the ith electron in the second undulator. Notice, that

$$\tau_i^{(2)} - \tau_i^{(1)} = \ell_i / v \tag{3}$$

where ℓ_i is the pathlength of the particle trajectory between two points and v is the particle velocity. According to the simulation results of the preceding section, the distribution function of the pathlengths of all beam particles can be described by a Gaussian probability function:

$$P(\ell_i) = \frac{1}{\sqrt{2\pi}\Delta\ell} \exp\left\{-\frac{(\ell_i - \ell_0)^2}{2\Delta\ell^2}\right\}, \tag{4}$$

where ℓ_0 is the average pathlength and $\Delta\ell$ is the rms deviation of the distribution.

We also assume a Gaussian distribution for the spectral function of the radiation intensity:

$$I(\omega) = \frac{c}{4\pi}\left\langle |E_1(\omega)|^2\right\rangle = \frac{c}{4\pi}\left\langle |E_2(\omega)|^2\right\rangle = \frac{I_0}{\sqrt{2\pi}\Delta\omega} \exp\left\{-\frac{(\omega - \omega_0)^2}{2\Delta\omega^2}\right\}, \tag{5}$$

where c is the speed of light, ω_0 is the central frequency and $\Delta\omega$ is the effective spectral bandwidth of the radiation field behind the filter of the measuring system.

By writing the Fourier transform of $e(t)$ in the form:

$$e(t) = \frac{1}{2\pi}\int_{-\infty}^{\infty} \hat{e}(\omega)\, e^{-i\omega t} dt, \tag{6}$$

and by plugging Eq's.(5) and (2) into Eq.(1), we get:

$$\gamma_{12}(\tau) = \sum_{i,j=1}^{N} \exp\left\{-\frac{\Delta\omega^2\left(\tau_j^{(2)} - \tau_i^{(1)} + \tau\right)^2}{2}\right\} \exp\left\{i\omega_0\left(\tau_j^{(2)} - \tau_i^{(1)} + \tau\right)\right\}. \qquad (7)$$

Since a reciprocal of $\Delta\omega$ is much shorter than the duration of the radiation pulse, we can neglect most of the terms with $j \neq i$ due to the first exponent in Eq.(7). Now, by averaging $\gamma_{12}(\tau)$ over the ensemble of particles with the probability function of Eq.(4), we get:

$$\overline{\gamma_{12}(\tau)} \simeq \exp\left\{-\frac{k^2\Delta\ell^2}{2}\right\} \exp\left\{-\frac{\Delta\omega^2\tau^2}{2}\right\} \exp\{i\omega_0\tau\}, \qquad (8)$$

where $k = \omega_o/c$ is the wave number.

The second exponent in Eq.(8) shows that the coherence drops with the characteristic time scale $1/\Delta\omega$. The first exponent in Eq.(8) shows the effect of imperfections. It shows that the coherence drops with increasing particle longitudinal mixing, $\Delta\ell$, during the beam passage between the two undulators.

We performed the simulation of the coherence of the fields of electron bunch radiation in the first and the second undulators with a 'brute-force' technique. In these simulations we assumed that the two undulators are identical and each undulator has ten undulator periods. The central wavelength of the radiation spectrum is 0.6μm. First, we model the radiation field $E_1(t)$ of the electron bunch radiation in the first undulator by taking a sum of the radiation fields of 10^4 electrons randomly distributed along the bunch with the uniform average longitudinal density. An example of such a field is shown in Figure (12a). Then, we reproduce the actual mixing of the longitudinal coordinates of electrons within the bunch that occurs during the bunch passage through the bypass lattice. We do this by randomly displacing each electron on the distance $(\ell_i - \ell_0)$ in such a way that the distribution of all distances $(\ell_i - \ell_0)$ taken over 10^4 electrons closely resembles the histogram in the previous section. Then, we model the radiation field $E_2(t)$ of the electron bunch radiation in the second undulator by taking a sum of the radiation fields of all 10^4 electrons with the new longitudinal positions that they get after the mixing. An example of this field is shown in Figure (12b). In this example we mixed electron longitudinal coordinates using the histogram in Figure (10b) as the reference distribution for a spread of the pathlengths. (This is a case when all kind of errors are present). By comparing Figure (12b) with Figure (12a) one can see changes in the radiation field that appeared due to the time-of-flight errors.

Finally, we calculated the correlation function of two radiation fields and plotted it in Figure (13). This correlation function characterizes the degree of coherence between the radiation fields of the electron beam radiation in the first and second undulators. As a reference function, in Figure (13b) we plotted the correlation function of two radiation fields for a case without mixing of the electron longitudinal coordinates, i.e. the correlation function of absolutely coherent fields. By comparing Figure (13a) with Figure (13b) we find that in the case with time-of-flight errors the degree of coherence drops by a factor of 5. Notice, that according to Eq.(8), this drop of the coherence should take place for

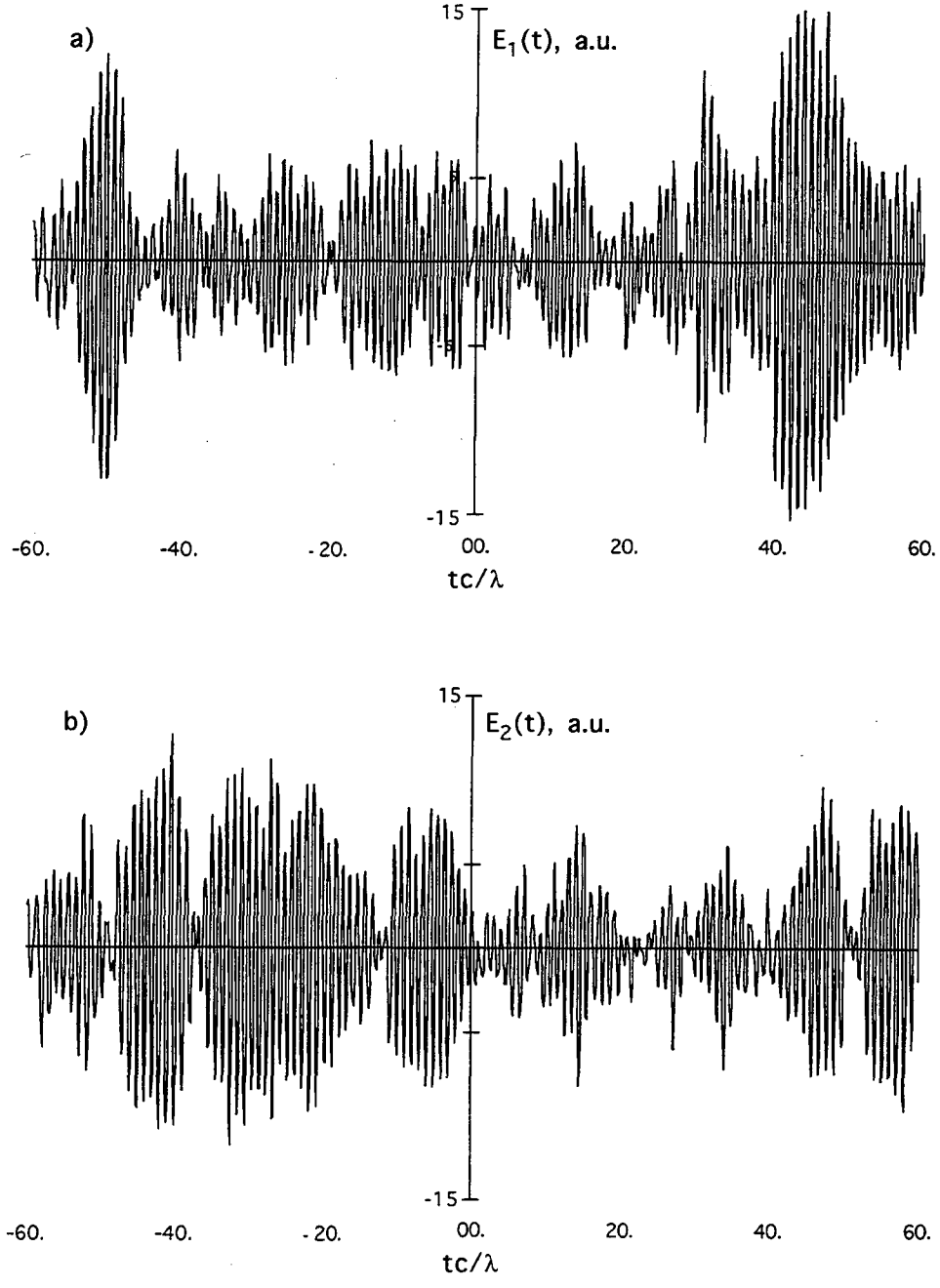

Figure 12: The field of the beam radiation in the undulator with ten periods: a) the radiation field $E_1(t)$, b) the radiation field $E_2(t)$. Only a short pattern of the field near the center of the radiation pulse is shown.

a Gaussian distribution of the spread of the pathlengths with $\sigma = 0.171$ micron (recall that $\lambda = 0.6\mu$m), which is in good agreement with the fitted result of $\sigma = 0.169$ micron at Figure (12b).

The analysis performed for a histogram shown in the Figure (11b) shows no traces of coherence (see, Figure (14)). This is not a surprise, because the spread of the pathlengths in this case has the rms deviation $\Delta\ell = 0.82\lambda$ and a reduction factor from the first exponent in the Eq.(8) is over 100.

In the anticipation that coupling of betatron oscillations in the Booster can be corrected, we also performed another set of simulations using six times smaller vertical emittance 1×10^{-8} m·rad and approximately one and a half times larger horizontal emittance 1.5×10^{-7} m·rad. These simulations showed that by reducing the vertical emittance we can get better coherence of undulator radiation fields. More specifically, the maximum of the coherence function γ_{12} rose to approximately 0.35.

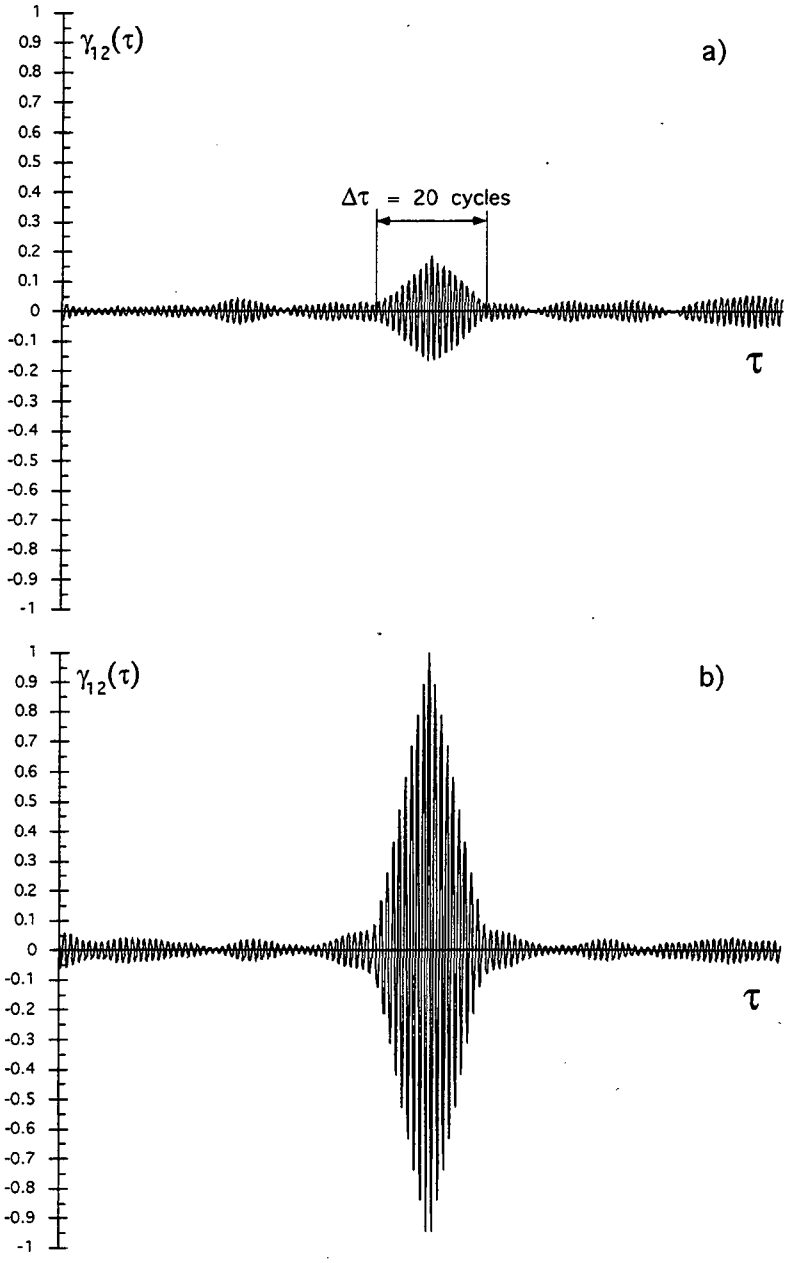

Figure 13: The correlation function of two radiation fields: a) a spread of the pathlengths has the rms deviation $\Delta\ell = 0.28\lambda$, b) zero mixing and absolutely identical radiation fields.

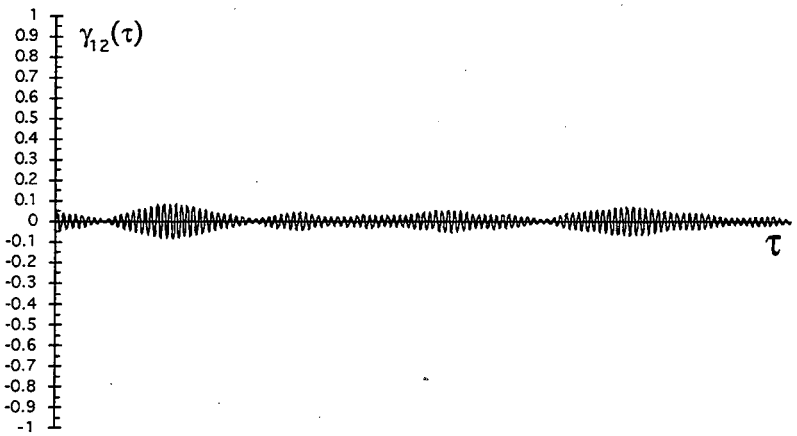

Figurè 14: The correlation function of two radiation fields for a case of a spread of the pathlengths with the rms deviation $\Delta\ell = 0.82\lambda$.

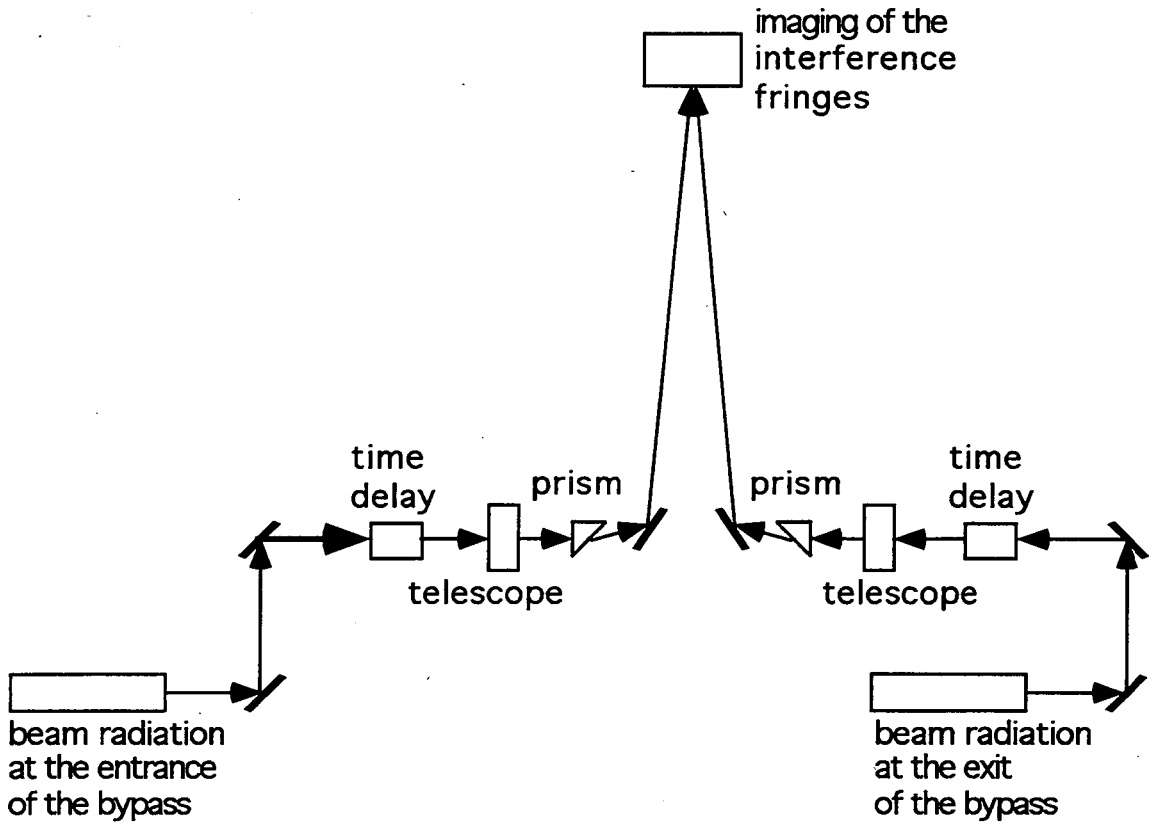

Figure 15: A schematic of the measurement of the interference fringes of two radiation fields.

7 Diagnostics

For the purpose of studying of the time-of-flight properties of the bypass beamline we do not really need to use undulators as a source of the beam radiation. An ordinary bend magnet can be used equally well. In this case a required bandwidth of the radiation signal of $\sim$ 10% can be provided by the filter. Behind the filter we will have a similar temporal structure of the radiation fields that is shown in Figure (12) for a case of the undulator radiation with 10 undulator periods. The only difference that will be found using bending magnets is approximately ten times less spectral density of the photon flux. The advantage of the bending magnets versus undulators is a significant cost saving (not to mention space saving that is also critical for the tiny area available at the ALS Booster synchrotron).

We anticipate to collect approximately 10^6 photons in $1/\gamma$ angle and 10% bandwidth per pulse of the radiation of 10^{10} electrons. This should be enough for observation of the interference fringes of two radiation fields on the CCD camera in a scheme shown in Figure (15). Moreover, 10 different spectral regions can be analyzed simultaneously in a single shot by utilizing color decomposition of the signal. Booster synchrotron operation

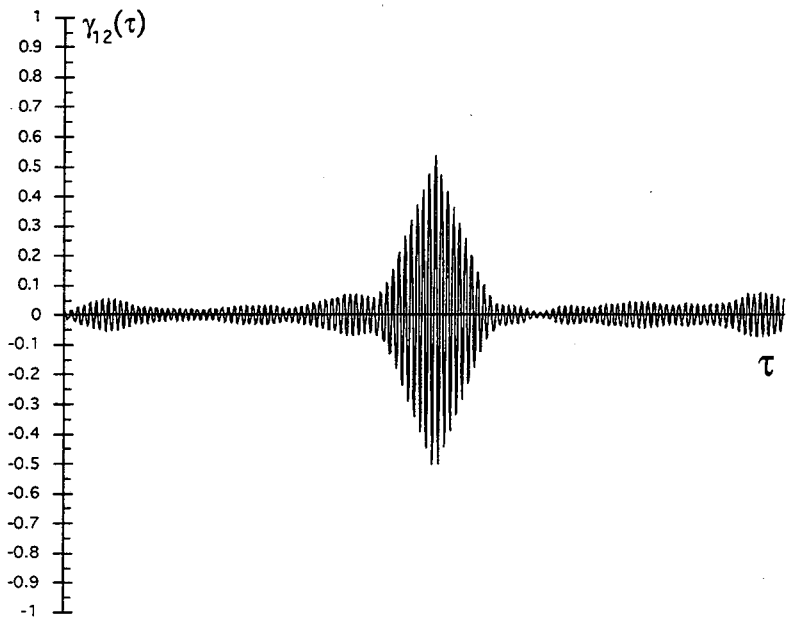

Figure 16: The correlation function of two radiation fields for measurements at $\lambda = 10\mu$m. No beam based tuning is assumed. The rms spread of the pathlengths is 1.9μm.

with the repetition rate of 1 Hz gives a sufficient time to download the data from every pulse.

During commissioning of the bypass we begin from a condition where a correlation function of two radiation fields would be much less sensitive to errors. Namely, if one can do measurements at $\lambda = 10\mu$m, then even without any additional tuning of the lattice and with the alignment errors of 250μm we would be able to observe the correlation function as it is shown in Figure (16). At the time of this writing it does not look feasible to do a single shot measurement of the correlation function of the radiation fields in the far infrared with commercially available infrared detectors. Instead, we will measure the intensity of the beam radiation behind the filter with a bandwidth that is approximately ten times wider than a reciprocal of the bunch pulse duration. If mixing of electrons within a bunch in the bypass is not too large compared to the central frequency of the bandwidth, then there must be a correlation of intensities of the radiation taken at the beginning and at the end of the bypass. It turns out that a correlator calculated for a large number of pulses is equal:

$$K \simeq \exp\left\{-k^2\Delta\ell^2\right\} \tag{9}$$

By doing measurements with fast infrared detectors, such as the HgCdTe detector, we would be able to collect a source radiation intensity that is above background thermal radiation.

8 Conclusion

We described a feasibility study of an experiment aimed at testing the Optical Stochastic Cooling technique in a single pass beam line installed in the extraction area of the ALS Booster synchrotron. Our conclusion is that this experiment can be performed as it is planed, thus providing an important experimental verification of the new beam cooling technique.

9 Acknowledgment

We are grateful to M. Fahmie, J. Johnson, K. Luchini and G. Jan De Vries for help in the modification of the energy ramp profile in the Booster synchrotron and A. Jackson for the interest to this work. The friendly assistance of the ALS Operations Staff for the emittance measurements is greatly appreciated.

References

[1] A. Mikhalichenko and M. Zolotorev, *Optical Stochastic Cooling*, Physical Review Letters, v.71, 25,1993, p.4146

[2] M. Zolotorev and A. Zholents, *Transit-time Method of Optical Stochastic Cooling*, Physical Review E, v.50, N4,1994, p.3087

[3] W. Wan, *Theory and Applications of Arbitrary-Order Achromats*, Ph.D. Thesis 1995, Michigan State University, University Microfilms, Inc., Ann Arber, MI; Technical Report MSUCL-976, NSCL/MSU, East Lansing, MI (1995)

[4] W. Wan and M. Berz, *An Analytic Theory of Arbitrary-Order Achromats*, Phys. Rev. E, in print

[5] K. L. Brown, D. C. Carey, Ch. Iselin and Rothacker, *TRANSPORT - A Computer Program for Designing Charged Particle Beam Transport Systems*, CERN 73-16, revised as CERN 80-4, CERN, 1980

[6] M. Berz, *COSY INFINITY Version 7 User's Guide and Reference Manual*, Technical Report MSUCL-977, National Superconducting Cyclotron Laboratory, Michigan State University, East Lansing, MI 48824, 1995

Ernest Orlando Lawrence Berkeley National Laboratory
One Cyclotron Road | Berkeley, California 94720

Prepared for the U.S. Department of Energy under Contract No. DE-AC03-76SF00098